Analyst

PAPER

View Article Online
View Journal | View Issue

Cite this: *Analyst*, 2019, **144**, 481

An electrochemical enzymatic nanoreactor based on dendritic mesoporous silica nanoparticles for living cell H_2O_2 detection†

Guangmin Bai,[a] Xuan Xu, *[a] Qumei Dai,[a] Qiqin Zheng,[a] Yuewei Yao,[a] Songqin Liu [b] and Cheng Yao [a]

Received 4th September 2018,
Accepted 25th October 2018

DOI: 10.1039/c8an01712c

rsc.li/analyst

The selective and quantitative detection of cellular H_2O_2 is essential for understanding its roles in physiology and pathology. A new electrochemical H_2O_2 biosensor, fabricated by immobilizing horseradish peroxidase onto dendritic mesoporous silica nanoparticles (HRP/DMSNs), is employed for living cell H_2O_2 detection. Taking advantage of the large pore volume and highly accessible internal surface areas of DMSNs, HRP/DMSNs display higher enzymatic loading, better stability and bioactivity in comparison with HRP on nonporous silica nanoparticles (NSNs). Therefore, a HRP/DMSN modified GCE (HRP/DMSNs/GCE) shows attractive electrochemical performance for sensitive and selective detection of H_2O_2 in 0.1 M pH 7.0 PBS, with a low K_m^{app} value of 11.48 μM and a low detection limit of 0.11 μM. In addition, HRP/DMSNs/GCE is successfully applied to detect H_2O_2 released from a PC12 cell triggered by ascorbic acid (AA). The detected H_2O_2 amount is close to the reported values. The developed biosensor has potential in the dynamic detection of the flux of H_2O_2 from living cells for further evaluation of oxidative stress in cells.

Introduction

Hydrogen peroxide (H_2O_2), a common representative of reactive oxygen species (ROS), is endogenously produced in living organisms and regulates various physiological processes.[1,2] It plays significant roles in reductive–oxidative-based signal transduction cascades and also acts as a rapid neuromodulatory signaling molecule to regulate the release of biomolecules.[3] However, an excessive amount of H_2O_2 accumulation in cells can lead to oxidative stress that causes various pathological events including cancer, neurodegeneration, cardiovascular, diabetes and atherosclerosis.[2] Therefore, the selective and quantitative detection of H_2O_2 in cells is essential for understanding its roles in cellular physiology. It can further assist in reliable diagnosis of pathological conditions.

Numerous analytical methods including titrimetry,[4] spectrophotometry,[5] chemiluminescence[6] and electrochemistry[7] have been developed to assay cellular H_2O_2. Among these methods, the electrochemical sensor based on redox proteins or enzymes (hemoglobin, horseradish peroxidase or cytochrome c) is an attractive tool.[8] It works at a sensing potential close to the potential of the redox protein to eliminate the interference reactions and simplify the detection system with less reagents.[9] However, natural enzymes are sensitive to the environmental conditions and the instability of enzyme-based biosensors is inevitable, which largely limits their further application in a complex cell environment.

Recently, enzymatic micro/nanoreactors have received considerable attention because of their applications in the evaluation of enzymatic reaction kinetics occurring inside nanospaces. Accumulated evidence has proved that enzyme confinement in an appropriate space can increase its catalytic activity and reduce denaturation by protein unfolding.[10–12] Some inorganic three-dimensional porous materials including porous graphene,[13] gold nanocages (AuNGs),[14] and porous carbon[15] have shown good performance in fabricating enzymatic nanoreactors, which largely improve the stability of confined enzymes and protect them from the external environment. Mesoporous silicas (MSs) are porous materials with pore sizes in the range of 2–50 nm.[16] Due to the excellent biocompatibility and the comparable pore size to the diameter of enzymes, MSs act as good candidates for enzymatic immobilization.[17,18] Recently, dendritic mesoporous silica nanoparticles (DMSNs) with center-radial oriented open and large mesopores have been invented as a new kind of MS.[19,20] Compared with conventional MSs, DMSNs have advantages of large pore volumes and highly accessible internal surface areas.[21,22] However, few

[a]College of Chemistry and Molecular Engineering, Nanjing Tech University, Nanjing 211816, P. R. China. E-mail: xuxuan0205@njtech.edu.cn; Fax: +86 25 58139527
[b]Jiangsu Province Hi-Tech Key Laboratory for Bio-medical Research, School of Chemistry and Chemical Engineering, Southeast University, Nanjing 211189, P. R. China

†Electronic supplementary information (ESI) available. See DOI: 10.1039/c8an01712c

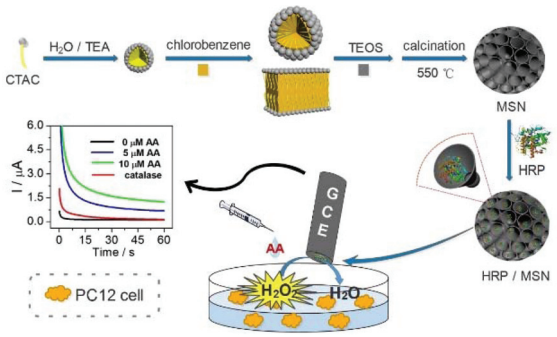

Scheme 1 Schematic of HRP/DMSN modified GCE used for detecting H_2O_2 efflux from cells stimulated with ascorbic acid (AA).

electrochemical enzymatic nanoreactors based on DMSNs have been fabricated for living cell H_2O_2 detection.

In this work, we developed a facile electrochemical H_2O_2 sensor based on DMSNs to measure the released H_2O_2 from living cells (Scheme 1). Firstly, DMSNs with a pore size of ~28 nm were synthesized by using the structure-directing agent of CTAC and the catalyst of TEA. After that, horseradish peroxidase (HRP) was adsorbed onto DMSNs (HRP/DMSNs) by electrostatic interaction at a pH value of 7.0. By spectroscopy and electrochemical methods, the loading efficiency and bioactivity of HRP confined in DMSNs were compared with that on nonporous silica nanoparticles (NSNs). In addition, the electrochemical biosensor was used for the selective detection of H_2O_2, both in 0.1 M pH 7.0 PBS and in the cell environment.

Experimental

Materials

Cetyltrimethylammonium chloride (CTAC) solution (25 wt% in H_2O), chlorobenzene (99.9%), tetraethyl orthosilicate (TEOS, >98%), naphthol (0.05 wt%), 3,3′,5,5′-tetramethylbenzidine (TMB) and horseradish peroxidase (HRP) were purchased from Sigma-Aldrich (Shanghai, China). Triethylamine (>99%), hydrogen peroxide solution (30 wt%), uric acid (UA), ascorbic acid (AA), dopamine (DA) and catalases (2000–5000 units per mL) were purchased from Beijing Chemical Reagent (Beijing, China). All chemicals were used as received without purification. 0.1 M phosphate buffer solution (PBS, pH 7.0) comprising NaH_2PO_4 and Na_2HPO_4 was used as the supporting electrolyte. A physiological PBS solution containing NaH_2PO_4 (1.76 mM), Na_2HPO_4 (10.14 mM), NaCl (136.75 mM), and KCl (2.28 mM) was mainly used for washing PC12 cells and observing the release of H_2O_2 from the cells. Other chemicals were all of analytical grade, and the solutions were prepared using doubly distilled water.

Apparatus

Transmission electron microscopy (TEM) images were obtained with a JEM-2100 (JEOL, Japan) electron microscope operating at 200 kV. Scanning electron microscopy (SEM) images were obtained on a Phenom ProX scanning electron microscope (The Netherlands). UV-vis absorption spectra were recorded with a PerkinElmer Lambda 35 spectrometer. Nitrogen adsorption–desorption measurements were conducted with a Micromeritcs Tristar II system (Tristar II 3020). Before testing, the samples were degassed at 323 K overnight on a vacuum line. The total pore volume was calculated from the amount adsorbed at a maximum relative pressure (P/P_0) of 0.99. The Barrett–Joyner–Halenda method was used to calculate the pore size of the samples from the adsorption branches of the isotherms. Zeta potential measurements were performed using a Zetasizer nano ZS (Malvern Instruments). Electrochemical measurements were performed on a CHI 832D workstation with a traditional three-electrode system including a modified glassy carbon electrode (GCE, d = 3 mm), a Pt wire and a saturated calomel electrode (SCE) as the working, auxiliary and reference electrodes, respectively.

Preparation of monodisperse mesoporous silica nanoparticles (DMSNs)

DMSNs were synthesized in a chlorobenzene–water system, using CTAC as the structure-directing agent, TEOS as the silica source, and TEA as the catalyst. In a typical synthesis, CTAC (25% water solution, 4.8 mL), TEA (0.04 g), and distilled water (7.2 mL) were mixed under vigorous stirring. Later, 4 mL of the oil phase (containing 3.5 mL chlorobenzene and 0.5 mL TEOS) were added to the water phase at 90 °C at a stirring speed of 500 RPM. DMSNs were collected by centrifugation after 12 h of stirring followed by calcination at 550 °C.[23,24]

Preparation of monodisperse nonporous silica nanoparticles (NSNs)

The monodisperse nonporous SiO_2 spheres were prepared by the well-known Stöber method. In brief, ethanol (80 mL), distilled water (4.85 mL) and ammonium hydroxide solution (25%, 3.6 mL) were added to a 250 mL flask, respectively. It was heated gradually to a certain temperature while under continuous stirring. Then, the mixed solution of TEOS (3.1 mL) and ethanol (8 mL) was added to the solution rapidly. Reaction occurred under continuous stirring over a period of 5 h at 55 °C. Colloid suspension SiO_2 nanoparticles were obtained. They were used as the seeds for the subsequent experiment on particle growth. For the seed-growth, 10 mL of the above colloid suspension was mixed with ethanol, distilled water and ammonium hydroxide solution in a 250 mL flask. Then, the mixture containing TEOS (1 mL) and ethanol (10 mL) was dropped into the flask slowly and stirred for another 5 h. This step was repeated several times to gain silica nanoparticles with a larger diameter.

Preparation of HRP/DMSN or HRP/NSN nanocomposites

Briefly, 10 mg DMSN or NSN powder was dispersed in 10 mL doubly distilled water by ultrasonication for 15 min. Then, 3 mg mL^{-1} HRP (10 μL) was mixed with 10 mg mL^{-1} DMSN or NSN suspension (20 μL) in 0.1 M pH 7.0 PBS. After vibration

with gentle shaking at room temperature overnight, free HRP was removed by centrifugation and washing with 0.1 M PBS several times to obtain the HRP/DMSN or HRP/NSN nanocomposites.

Preparation of HRP/DMSN and HRP/NSN modified GCE

To investigate the electrochemical properties of HRP immobilized on DMSNs or NSNs, modified electrodes were assembled as follows. Prior to being used, GCE was polished with 0.3 and 0.05 μm alumina slurry, and sonicated in ethanol and water successively. Then, 10 μL of HRP/DMSN or HRP/NSN aqueous solution was dropped on the pretreated GCE and dried in a desiccator. After being dried, 10 μL of Nafion solution (0.05%) was dropped onto the surface and dried to obtain HRP/DMSN or HRP/NSN modified GCE. Finally, the modified electrodes were kept at 4 °C before use.

Evaluation of enzymes immobilized on DMSNs or NSNs

The amount of HRP immobilized on DMSNs or NSNs was determined by the Bradford method.[23] Briefly, 3 mg mL^{-1} HRP solution (10 μL) was mixed with 10 mg mL^{-1} DMSN or NSN suspension (20 μL). The mixture was vibrated at room temperature with gentle shaking for 24 h, and subjected to centrifugation. The collected supernatant solution was added to 5 mL of Coomassie Brilliant Blue G-250 (CBB, 0.1 g L^{-1} in water) and incubated for 30 minutes. The residual protein concentration was measured using the calibration curve of HRP standard solution by monitoring the absorbance at 595 nm. Thus, the loading capacity was calculated as follows:

$$\text{Loading capacity}(\text{mg g}^{-1}) = \frac{\text{initial enzyme amount}(\text{mg}) - \text{residual enzyme amount}(\text{mg})}{\text{the amount of MSNs material}(\text{g})}.$$

The loading experiment was repeated 3 times.

Selective removal of externally adsorbed proteins and activity assay

A solution comprising HRP/DMSN bioconjugates (80 μL) with 5 M NaCl aqueous solution (20 μL) was shaken for 5 min. After that, the mixture was gently centrifuged twice to remove any unbound protein and re-dispersed in 50 μL of pH 7.4 PBS. Thereafter, the centrifuged supernatants were subjected to the activity assay with the addition of H_2O_2 and TMB chromogenic solution. After standing for 1 min at room temperature, the enzymatic reaction was terminated with 100 μL of 1 mM sulfuric acid and measured on a UV-vis spectrophotometer.

Detection of H_2O_2 released from living cells

The HRP/DMSN/GCE electrode was explored for the detection of released H_2O_2 in living cells. Rat pheochromocytoma (PC12) cells were chosen as the model cell line and obtained from KeyGene Biotechnology Co., Ltd (Jiangsu, China). PC12 cells were grown in a 24-well plate and incubated at 37 °C for hours. After that, they were collected by centrifugation, washed three times with deoxygenated PBS (pH 7.0), and then 3 mL of deoxygenated PBS was added for real sample measurements. The cell number was estimated by using a hemocytometer and the number is 6×10^6. The H_2O_2 release was triggered by injecting ascorbic acid (AA) and a conventional three-electrode system was adopted for the electrochemical experiment. During the test, the HRP/DMSN/GCE electrode was applied at the potential of −0.4 V (*vs.* SCE) and exposed to the cell solution. As a control experiment, 400 U mL^{-1} of catalase (2000–5000 units per mL) was then added to the solution that contained cells.

Results and discussion

Characterization of DMSNs

DMSNs were synthesized according to Xu's method with minor modification (Scheme 1).[25] The morphology and microstructure of DMSNs were characterized by scanning electron microscopy (SEM) and transmission electron microscopy (TEM). The SEM image in Fig. 1A shows that all DMSNs are spherical in shape with a uniform particle size and porous morphology on the surface. Calculated by 80 particles, the average diameter of DMSNs is ~122 nm with the relative standard deviation (RSD) of 8.52%. With dynamic light scattering (DLS) measurements, the *z*-average diameter of DMSNs in deionized (DI) water is determined to be 150 nm (Fig. S1†), which is slightly larger than the size calculated from the SEM image. This is because the DLS measurement represents the hydrodynamic diameter of the particle including surrounding water molecules.[26] TEM images in Fig. 1B and C display that

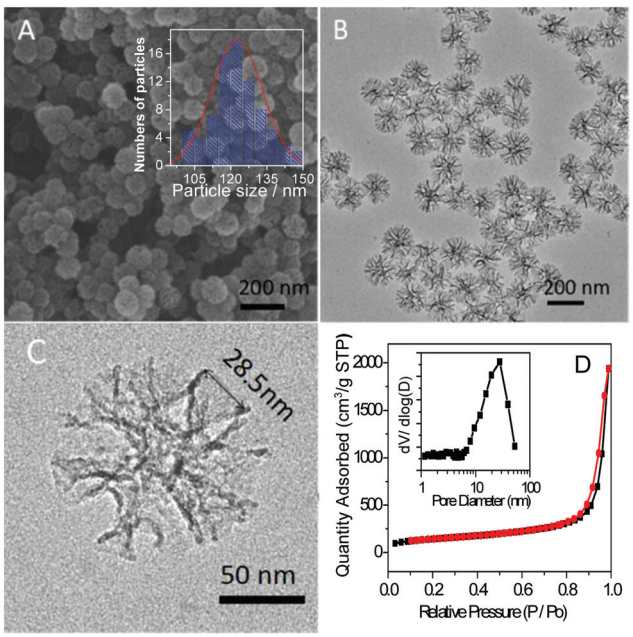

Fig. 1 (A) Scanning electron microscopy (SEM) image of DMSNs. Insert: the size distribution of DMSNs fitted by the Gaussian function. (B, C) Transmission electron micrographs of DMSNs. (D) N_2 adsorption/desorption isotherm. Inset: pore size distribution curve of DMSNs.

DMSNs have a flower-like structure with many cone-like petals formed by silica lamellae attached to the central core. The detailed structure of the cores and the cone walls can also be clearly distinguished. All the silica cones have open ends that are advantageous for further adsorption of enzymes.

The pore size, pore volume and surface area of DMSNs were further characterized by nitrogen sorption analysis (Fig. 1D). The nitrogen-adsorption–desorption plot of DMSNs gives a type IV isotherm and a steep capillary condensation step occurring at a relative pressure (P/P_0) of ≈0.88. In the inset of Fig. 1D, the corresponding Barrett–Joyner–Halenda (BJH) pore size distribution curve derived from the adsorption branch of the isotherm displays a well-defined peak centered at ~28 nm. Furthermore, the Brunauer–Emmett–Teller surface area of DMSNs is calculated to be 512 m^2 g^{-1} and the total pore volume is 3.002 cm^3 g^{-1} at P/P_0 = 0.988. Their pore volume value is comparable to 0.7 cm^3 g^{-1} of XL-DMSNs with a pore size of 30 nm.[27] It is also larger than 0.57 cm^3 g^{-1} of multilamellar silica vesicles with a pore size of 2.6 nm.[28] Such a high pore volume of DMSNs is consistent with their large pore size and thin wall thickness.

The surface charge properties of DMSNs were analyzed by zeta potential measurements. DMSNs display a negative surface charge with a zeta potential value of −24.7 ± 4 mV in PBS. At the same time, HRP has a net positive charge in the medium solution at a neutral pH value because the isoelectric point of HRP is 9.[29] Therefore, HRP can be adsorbed onto DMSNs by electrostatic interaction when the pH value is 7.0. To test the loading capacity of HRP in mesoporous silica, Bradford method analysis was employed and calculated by using the formula shown in the Experimental section.[29] In this work, the loading capacity is calculated as the adsorbed amount of proteins per g of silica nanoparticles. Coomassie blue is used to measure the protein load by UV-vis spectroscopy (Fig. S3†). As shown in Table S1,† the loading capacity of HRP on DMSNs is 23.6 mg g^{-1}. For comparison, the loading capacity of HRP on NSNs (the average diameter of ~120 nm) is also tested and the loading capacity is 8.12 mg g^{-1}. Obviously, the loading capacity of HRP on DMSNs is ~2.9 times larger than that on NSNs, which is attributed to the large surface area and high pore volume of porous DMSNs. However, HRP can be adsorbed on the internal and external surfaces of DMSNs. To study the influence of externally adsorbed proteins, a high salt concentration (1 M NaCl) buffer is used for selective removal of external proteins.[14] The catalytic activities of HRP/DMSNs before and after the treatment of high salt solution are compared in Fig. S4.† It shows that the removal of external HRP only decreases the activity of HRP/DMSNs by ~7%. Therefore, the externally immobilized enzymes on DMSNs can be negligible, and the catalytic activity of HRP/DMSNs is mainly ascribed to HRP confined in the pores.

Direct electrochemistry of HRP/DMSNs/GCE

Fig. 2A shows the cyclic voltammetry of different modified electrodes carried out in nitrogen-saturated PBS at a scan rate of 100 mV s^{-1}. HRP/DMSNs/GCE (curve a) gives a couple of

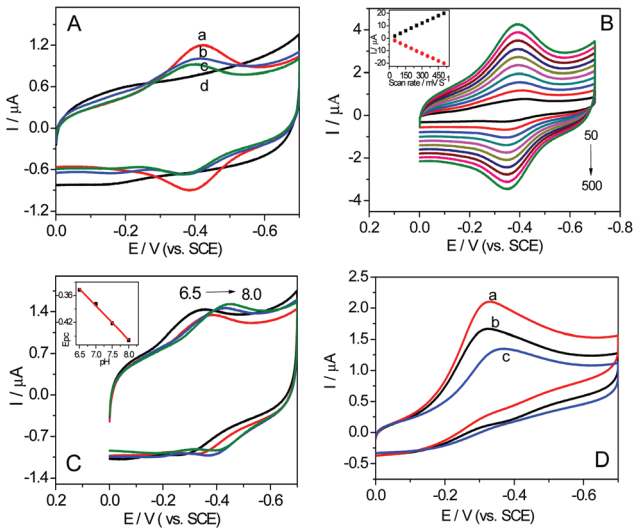

Fig. 2 (A) CV curves of HRP/DMSNs/GCE (a), HRP/NSNs/GCE (b), HRP/GCE (c) and DMSNs/GCE (d) in anaerobic 0.1 M pH 7.0 PBS at a scan rate of 100 mV s^{-1}. (B) CV curves of HRP/DMSNS/GCE in anaerobic PBS at different scan rates. (C) CV curves of HRP/DMSNs/GCE in anaerobic PBS with pH values of 6.5, 7.0, 7.5 and 8.0. (D) CV curves of HRP/DMSNs/GCE (a), HRP/NSNs/GCE (b) and HRP/GCE (c) in anaerobic 0.1 M pH 7.0 PBS containing 40 μM H_2O_2.

well-defined redox peaks at −0.423 V and −0.385 V, while no peaks are observed on the DMSNs/GCE (curve d) in the same potential window. It confirms that the redox response results from the direct electronic communication between HRP and the electrode.[30] The small peak-to-peak separation values indicate a fast electron transfer rate. According to Laviron's method,[31] the electron transfer rate constant k_s was estimated to be 19.46 s^{-1}. The effect of scan rate upon the voltammetric response of HRP/DMSN modified GCE was then studied (Fig. 2B). The plot of the anode and cathodic peak current *versus* the scan rate (insert of Fig. 2B) illustrates that the peak current increases linearly with the scan rates, suggesting the surface-controlled electrode process of the direct electron transfer. Electron transfer in biological systems is often accompanied by proton movement. Fig. 2C shows the cyclic voltammograms of HRP/DMSNs/GCE in 0.1 M PBS with different pH values of 6.5, 7.0, 7.5 and 8.0. The increase of pH causes a negative shift of the formal potential with the linear equation as E (V) = (−0.075) pH + 0.1478 (R^2 = 0.996). The slope of −75 mV per pH unit is close to the theoretical value for the reversible one-electron-transfer coupled with single-proton transportation (−58 mV pH^{-1} at 25 °C).

For comparison, the cyclic voltammetry of HRP/NSNs/GCE and HRP/GCE is carried out under the same conditions (curves b and c in Fig. 2A) and their corresponding electrochemical parameters are compared with HRP/DMSNs/GCE in Table S1.† It displays that there is no significant difference in the formal potential on the three modified electrodes. However, the electroactive amount (proportional to the measured charge) of HRP/DMSNs/GCE is almost 2.15 times

larger than HRP/NSNs/GCE and 2.32 times larger than HRP/GCE, which is consistent with the higher loading HRP capacity of the HRP/DMSNs. Furthermore, the biggest k_s value of HRP/DMSNs/GCE among the three modified electrodes indicates the good electrochemical response of HRP confined in DMSNs. It is ascribed to the good biocompatibility of the silica shell, which can retain the native structure of the enzyme. Besides, the mesoporous tunnels of the silica nanospheres help to accelerate the electron transfer between confined HRP and the electrode.[32]

Electrocatalytic response and calibration curve for H_2O_2 detection

The electrocatalytic behavior of H_2O_2 on HRP/DMSNs/GCE was further studied. Prior to detection, the electrolyte was bubbled with high purity nitrogen for the removal of the oxygen dissolved in the electrolyte. Curve a in Fig. 2D shows the CV curve of HRP/DMSNs/GCE in anaerobic 0.1 M pH 7.0 PBS containing 40 μM H_2O_2. The presence of H_2O_2 increases the reduction current dramatically, accompanied by a decrease and disappearance of the oxidation peak. It indicates the good electrocatalytic activity of the entrapped HRP on DMSNs towards H_2O_2. For comparison, the electrocatalytic behavior of HRP/GCE and HRP/NSNs/GCE was also studied under the same conditions. The catalytic currents on HRP/GCE and HRP/NSNs/GCE are 60.1% and 62.3% of that on HRP/DMSNs/GCE, respectively. The poor current responses result from the smaller amount of immobilized enzyme and the easy loss of bioactivity on the bare electrode surface.

Fig. 3A displays the CV curve of HRP/DMSNs/GCE in anaerobic 0.1 M PBS with different H_2O_2 concentrations. Once H_2O_2 was added to PBS, intense stirring was continued for more than 30 s. The reduction peak current on HRP/DMSNs/GCE increases with the increasing H_2O_2 concentration. As shown in Fig. 3B, the H_2O_2 sensor shows two segments of a linear range. The linear regression equation for the lower concentration (0.5 μM to 3 μM) is I_p (μA) = 0.857 + 0.113 $C_{H_2O_2}$ (μM) (R^2 = 0.991) with a sensitivity of 113 μA mM^{-1}. Another linear regression equation for the higher concentration (8 μM to 103 μM) is I_p (μA) = 1.062 + 0.0351 $C_{H_2O_2}$ (μM) (R^2 = 0.989) with a sensitivity of 35.1 μA mM^{-1}. The detection limit is estimated to be 0.11 μM (ratio of signal to noise, S/D = 3). At the same time, the calibration curve for H_2O_2 detection on HRP/NSNs/GCE is shown in Fig. S5.† One linear range is from 0.5 μM to 3 μM with a sensitivity of 54.5 μA mM^{-1}. Another linear range is from 3 μM to 68 μM with a sensitivity of 19.1 μA mM^{-1}. The detection limit is estimated to be 0.28 μM (S/D = 3). Obviously, the sensitivity of HRP/DMSNs/GCE is about 2 times larger than that of HRP/NSNs/GCE in the two linear ranges and the detection limit of HRP/DMSNs/GCE is also lower than that of HRP/NSNs/GCE. Furthermore, a comparison of the linear range and the detection limit of HRP/DMSNs/GCE with other H_2O_2 sensors reported in the literature is summarized in Table S2.† Compared with previous reports, the HRP/DMSNS/GCE biosensor possesses better performances with the lowest detection limit for the detection of H_2O_2.

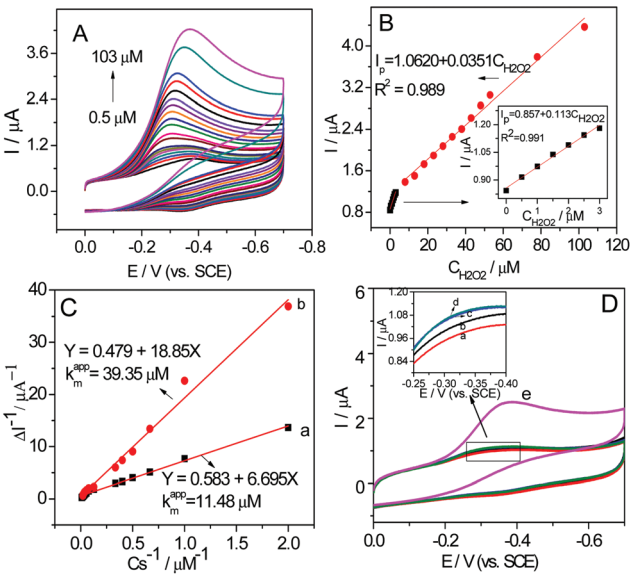

Fig. 3 (A) CV curves of HRP/DMSNs/GCE in anaerobic 0.1 M pH 7.0 PBS containing different concentrations of H_2O_2. (B) Plot of the cathodic peak currents *vs.* the concentrations of H_2O_2. (C) Double-reciprocal plot of the cathodic peak currents and the concentrations of H_2O_2 on HRP/DMSNs/GCE (a) and HRP/NSNs/GCE (b). (D) Cyclic voltammetry response of HRP/DMSNs/GCE without (a) and with the successive addition of 0.2 mM AA (b), 0.2 mM DA (c), 0.2 mM UA (d) and 40 μM H_2O_2 (e) to 0.1 M pH 7.0 PBS.

The apparent Michaelis–Menten constant (K_m^{app}), an indication of the enzyme–substrate kinetics, is generally used to evaluate the bioactivity of immobilized enzymes. The K_m^{app} value can be calculated by using the Lineweaver–Burk equation.[33]

$$\frac{1}{I_{ss}} = \frac{1}{I_{max}} + \frac{K_m}{I_{SS}C}$$

where I_{ss} is the steady-state current after the addition of the substrate, I_{max} is the maximum current in saturated substrate solution and C is the bulk concentration of the substrate. According to the slope and intercept from the double-reciprocal plot of catalytic currents and H_2O_2 concentrations (Fig. 3C), the K_m^{app} value on HRP/DMSNs/GCE is calculated to be 11.48 μM, which is close to 13.4 μM for HRP encapsulated in LCA nanotubes.[34] This K_m^{app} value is smaller than the sensors of HRP/GCE (43.14 μM) (Fig. S6†), HRP/NSNs/GCE (39.35 μM) and HRP/peptides/GCE (401 μM).[35] The lower K_m^{app} value indicates the higher enzymatic activity of immobilized HRP on DMSNs and higher affinity towards H_2O_2.

Anti-interference, reproducibility and stability of HRP/DMSNs/GCE

The anti-interference, reproducibility and stability of HRP/DMSNs/GCE were also evaluated. Firstly, the selectivity of the proposed biosensor against the most commonly existing interferences in the physiological environment was evaluated. Fig. 3D illustrates the cyclic voltammogram of HRP/DMSNs/

GCE upon successive addition of 0.2 mM AA, 0.2 mM DA, 0.2 mM UA and 40 μM H_2O_2. No obvious current response is observed after the injection of coexisting species, while a remarkable current response is generated with the addition of H_2O_2. It highlights the superior selectivity of the HRP/DMSN/GCE biosensor toward H_2O_2.

The stability and reproducibility of HRP/DMSNs/GCE were further investigated by measuring its response to 20 μM H_2O_2. As shown in Fig. S7,† four independent HRP/DMSN modified electrodes display a deviation of 9.4% (RSD) for the sensitivity to H_2O_2, indicating the acceptable reproducibility. When the as-prepared HRP/DMSNs/GCE was stored in a refrigerator at 4 °C for half a month, ~88% of the initial current response was retained.[36] These results prove that HRP/DMSNs/GCE displays high anti-interference, reproducibility and stability for determining H_2O_2, which are essential characteristic features of a sensor for practical application.

Detection of H_2O_2 released from living cells

H_2O_2 plays important roles in many biological processes *in vivo* and has been reported as a potential marker for tumor.[37,38] In this work, the developed H_2O_2 sensor (HRP/DMSNs/GCE) was utilized for the real-time detection of H_2O_2 released from cells. Taking the PC12 cell as an example, AA is employed as a stimulating agent to induce the generation of H_2O_2 from living cells.[39,40] Fig. 4A shows the CV curves obtained at HRP/DMSNs/GCE under different conditions. Curve a describes the response of HRP/DMSNs/GCE in the presence of PC12 cells. Its reduction current is obviously higher than that in blank PBS (curve a in Fig. 2A), which illustrates that HRP/DMSNs/GCE is able to sensitively detect ROS generation from tumour cells.[13] It further raises the possibility of the *in situ* quantitative detection of the released H_2O_2 from living cells by artificial stimulation. After the addition of AA, an obvious change in the current signal is observed and the reduction current increases with the injection of AA. However, no current change is observed after the addition of AA into PBS without cells (curve b in Fig. 3D). To confirm whether the increased current signal is caused by H_2O_2 produced from the stimulated cells, another experiment is carried out by adding catalase, which is a selective scavenger of H_2O_2. As shown in Fig. 4B, the reduction currents at −0.4 V increase by successive addition of AA to the solution containing living cells. However, after the injection of catalase, the current response decreases to its background level due to the specific disintegration decomposition of H_2O_2. This suggests that the amperometric responses are attributed to the electrochemical reduction of H_2O_2 released by living cells. According to the standard curve in Fig. 3B and the generated currents in Fig. 4A, the flux of H_2O_2 is estimated to be about 12 μM (in 2 mL PBS) when 6×10^6 PC12 cells are treated with 5 μM AA. The released amount of H_2O_2 in our work is close to the reported values.[40,41] It demonstrates that the HRP/DMSNs/GCE biosensor can be used for the detection of H_2O_2 released from the cells and its potential uses can be exploited for physiological and pathological studies.

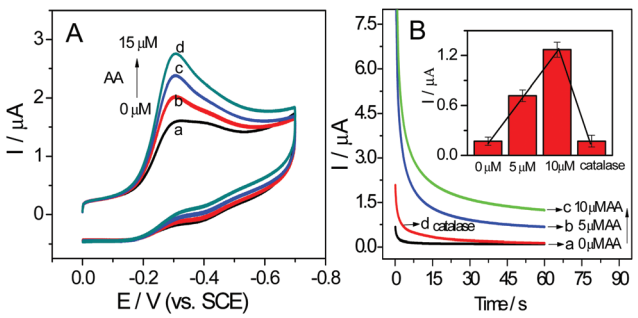

Fig. 4 (A) CV curves of HRP/DMSNs/GCE in anaerobic 0.1 M pH 7.0 PBS containing PC12 cells without (a) and with the addition of 5 μM AA (b), 10 μM AA (c) and 15 μM AA (d). (B) Amperometric responses of HRP/DMSNs/GCE at −0.4 V for the reduction of H_2O_2 released from neutrophils induced by AA without (b) and with the addition of 25 μL of catalase (400 U mL^{-1}) (d).

Conclusion

In summary, a novel HRP bioreactor is fabricated by immobilizing HRP on DMSNs (pore size of ~28 nm) with high HRP loading and easily accessible dendritic pore channels for substrates. Compared with HRP on nonporous silica nanoparticles, HRP/DMSNs show higher loading efficiency and better catalysis for H_2O_2. Accordingly, the electrochemical biosensor based on HRP/DMSNs exhibits attractive performance for sensitively and selectively detecting H_2O_2 with a wide linear detection range and low detection limit. Furthermore, the HRP/DMSNs/GCE biosensor has displayed great possibility of applications in the measurement of H_2O_2 released from the living cells, which is meaningful for evaluating oxidative stress of different kinds of cancer cells in clinical diagnostics.

Conflicts of interest

There are no conflicts of interest to declare.

Acknowledgements

We appreciate the financial support from the National Natural Science Foundation of China (Grants: 21505071), the Natural Science Foundation of Jiangsu Province (Grant: BK20150937) and the Jiangsu Government Scholarship for Overseas Studies (JS-2017-043).

References

1 R. Weinstain, E. N. Savariar, C. N. Felsen and R. Y. Tsien, *J. Am. Chem. Soc.*, 2014, **136**, 874–877.

2 H. X. Dai, W. J. Lu, X. W. Zuo, Q. Zhu, C. Pan, X. Y. Niu, J. J. Liu, H. L. Chen and X. G. Chen, *Biosens. Bioelectron.*, 2017, **95**, 131–137.
3 M. V. Avshalumov, J. C. Patel and M. E. Rice, *J. Neurophysiol.*, 2008, **100**, 1590–1601.
4 A. Brestovisky and E. K. Eisner, *Anal. Chem.*, 1983, **55**, 2063–2066.
5 R. F. Nogueira, M. C. Oliveira and W. C. Paterlini, *Talanta*, 2005, **66**, 86–91.
6 F. Ghavamipour, R. H. Sajedi and K. Khajeh, *Microchim. Acta*, 2018, **185**, 376.
7 Z. H. Bai, G. Y. Li, J. T. Liang, J. Su, Y. Zhang, H. Z. Chen, Y. Huang, W. G. Sui and Y. X. Zhao, *Biosens. Bioelectron.*, 2016, **82**, 185–194.
8 P. Wu, Z. W. Cai, Y. Gao, H. Zhang and C. X. Cai, *Chem. Commun.*, 2011, **47**, 11327–11329.
9 G. H. Zhang, N. B. Yang, Y. L. Ni, J. Shen, W. B. Zhao and X. H. Huang, *Sens. Actuators, B*, 2011, **158**, 130–137.
10 X. D. Cao, Y. Li, Z. Q. Zhang, J. C. Yu, J. Qian and S. Q. Liu, *Analyst*, 2012, **137**, 5785–5791.
11 J. C. Yu, Y. J. Zhang and S. Q. Liu, *Biosens. Bioelectron.*, 2014, **55**, 307–312.
12 Z. Zhou and M. Hartmann, *Chem. Soc. Rev.*, 2013, **42**, 3894–3912.
13 Y. D. Liu, X. H. Liu, Z. P. Guo, Z. G. Hu, Z. H. Xue and X. Q. Lu, *Biosens. Bioelectron.*, 2017, **87**, 101–107.
14 X. Qian, U. Rameshbabu, J. S. Dordick and R. W. Siegel, *Biomaterials*, 2016, **75**, 305–312.
15 W. B. Wei, S. Y. Dong, G. Q. Huang, Q. Xie and T. L. Huang, *Sens. Actuators, B*, 2018, **260**, 189–197.
16 C. T. Kresge, M. E. Leonowicz, W. J. Roth, J. C. Vartuli and J. S. Beck, *Nature*, 1992, **359**, 710–712.
17 Y. J. Wang and F. Caruso, *Chem. Mater.*, 2005, **17**, 953–961.
18 X. D. Cao, J. C. Yu, Z. Q. Zhang and S. Q. Liu, *Biosens. Bioelectron.*, 2012, **35**, 101–107.
19 D. K. Shen, J. P. Yang, X. M. Li, L. Zhou, R. Y. Zhang, W. Li, L. Chen, R. Wang, F. Zhang and D. Y. Zhao, *Nano Lett.*, 2014, **14**, 923–932.
20 P. C. Liu, Y. J. Yu, B. Peng, S. Y. Ma, T. Y. Ning, B. Q. Shan, T. Q. Yang, Q. S. Xue, K. Zhang and P. Wu, *Green Chem.*, 2017, **19**, 5575–5581.
21 D. Kwon, B. G. Cha, Y. Cho, J. Min, E. B. Park, S. J. Kang and J. Kim, *Nano Lett.*, 2017, **17**, 2747–2756.
22 A. K. Meka, P. L. Abbaraju, H. Song, C. Xu, J. Zhang, H. W. Zhang, M. H. Yu and C. Z. Yu, *Small*, 2016, **37**, 5169–5177.
23 C. Xu, M. H. Yu, O. Noonan, J. Zhang, H. Song, H. W. Zhang, C. Lei, Y. T. Niu, X. D. Huang, Y. N. Yang and C. Z. Yu, *Small*, 2015, **44**, 5949–5955.
24 M. M. Bradford, *Anal. Biochem.*, 1976, **72**, 248–254.
25 R. Frost, C. Langhammerb and T. Cedervallc, *Nanoscale*, 2017, **9**, 3620–3628.
26 D. Kwon, B. G. Cha, Y. Cho, J. Min, E. B. Park, S. J. Kang and J. Kim, *Nano Lett.*, 2017, **17**, 2747–2756.
27 J. Lu, Y. Zhang, H. Li, J. Yu and S. Liu, *Chem. Commun.*, 2014, **50**, 13896–13899.
28 A. S. Brown, A. L. Acton, J. A. Preece, J. S. Fossey and P. M. Mendes, *Chem. Sci.*, 2015, **6**, 5114–5119.
29 Y. K. Gao, W. Q. Zhu, J. Liu, D. H. Di, D. Chang, T. Y. Jiang and S. L. Wang, *Int. J. Pharm.*, 2015, **485**, 25–30.
30 X. Q. Liu, R. Yan, J. M. Zhang, J. Zhu and D. K. Y. Wong, *Biosens. Bioelectron.*, 2015, **66**, 208–215.
31 E. Laviron, *J. Electroanal. Chem.*, 1979, **101**, 19–28.
32 Z. Dai, J. Bao, X. Yang and H. Ju, *Biosens. Bioelectron.*, 2008, **23**, 1070–1076.
33 R. A. Kamin and G. S. Wilson, *Anal. Chem.*, 1980, **52**, 1198–1205.
34 Q. Lu, Y. Kim, N. Bassim, N. Raman and G. E. Collins, *Analyst*, 2016, **141**, 2191–2198.
35 X. Q. Liu, H. Q. Feng, J. M. Zhang, R. X. Zhao, X. H. Liu and D. K. Y. Wong, *Biosens. Bioelectron.*, 2012, **32**, 188–194.
36 H. R. Burachaloo, F. Karimi, K. Xie, Q. Fu, P. A. Gurr, D. E. Dunstan and G. G. Qiao, *ACS Appl. Mater. Interfaces*, 2017, **9**, 33599–33608.
37 X. L. Sun, S. J. Guo, Y. Liu and S. H. Sun, *Nano Lett.*, 2012, **12**, 4859–4863.
38 F. Xiao, Y. Q. Li, X. L. Zan, K. Liao, R. Xu and H. W. Duan, *Adv. Funct. Mater.*, 2012, **22**, 2487–2494.
39 Y. Zhang, C. Y. Wuang, X. J. Zhou, X. C. Wu, Y. Q. Yang, H. X. Wu, S. W. Guo and J. Y. Zhang, *Nanoscale*, 2013, **5**, 1816–1819.
40 J. Zhao, Y. L. Yan, L. Zhu, X. X. Li and G. X. Li, *Biosens. Bioelectron.*, 2013, **41**, 815–819.
41 Y. Zhang, X. Bai, X. Wang, K. K. Shiu, Y. Zhu and H. Jiang, *Anal. Chem.*, 2014, **86**, 9459–9465.